Synthesis of carbon-dots@SiO$_2$@TiO$_2$ nanoplatform for photothermal imaging induced multimodal synergistic antitumor

Bing Wei [a], Fei Dong [a], Wei Yang [c], Chunhua Luo [a], Qiujing Dong [a], Zuoqin Zhou [a], Zheng Yang [a,b,*], Liangquan Sheng [a,*]

[a] School of Chemistry and Materials Engineering, Engineering Research Center of Biomass Conversion and Pollution Prevention of Anhui Educational Institutions, Fuyang Normal University, Fuyang 236037, PR China
[b] AnHui Province Key Laboratory of Chemistry for Inorganic/Organic Hybrid Functionalized Materials, Anhui University, Hefei 230601, PR China
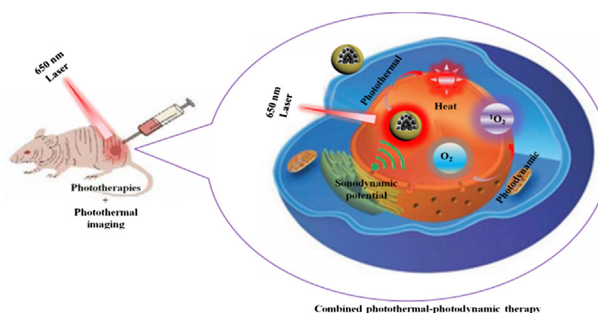[c] Anhui Chemical Engineering School, Anqing 246300, PR China

HIGHLIGHTS

- Multifunctional carbon dot@SiO$_2$@TiO$_2$ nanoplatforms (CST NPs) were firstly fabricated.
- The CST NPs possessed outstanding photodynamic ability by fluorescence resonance energy transfer effect.
- The synthesized CST NPs achieved synergetic PTT and enhanced PDT both *in vitro* and *in vivo*.
- The photothermal imaging property of CST NPs endowing real-time phototheranostics for tumor *in vivo*.

GRAPHICAL ABSTRACT

A nanoplatform could perform excellent photothermal therapy and fluorescence resonance energy transfer induced photodynamic therapy for real-time photothermal imaging guided synergistic phototherapy of cancer.

ARTICLE INFO

ABSTRACT

For facilitating theranostic nanoplatform with multimodal therapeutic ability, we develop the core-shell structured CDs@SiO$_2$@TiO$_2$ nanoplatforms (CST NPs). The designed CST NPs possess excellent photothermal effect and fluorescence resonance energy transfer (FRET) induced photodynamic property, which could achieve synergistic photothermal and photodynamic therapy. Meanwhile, the photothermal ability of CST NPs acts as a key role in the application of real-time photothermal imaging, benefitting for the diagnosis of tumor accurately. Moreover, the obtained CST NPs also exhibit outstanding sonodynamic effect with huge potential for sonodynamic therapy. Under the 650 nm laser irradiation, the synthesized CST NPs not only inhibit the growth of cancer cells *in vitro*, but also display precise photothermal imaging and photo-induced ablation to tumor *in vivo*. As a result, the prepared CST NPs may potentially serve as multifunctional nanoplatform for theranostic antitumor and pave the avenue for clinic cancer therapy.
© 2020 The Authors. Published by Elsevier B.V. on behalf of Cairo University. This is an open access article under the CC BY-NC-ND license (http://creativecommons.org/licenses/by-nc-nd/4.0/).

Introduction

Due to the massive lacks of traditional cancer therapies, the clinic treatments for cancer are facing extensive challenges which include toxic side effect, low specifity, and huge invasion [1]. Recently, phototherapies such as photothermal therapy (PTT) and photodynamic therapy (PDT) attract abundant attentions of scientists possessing the advantages of non-invasion, excellent selectivity, and low toxicity [2]. However, PTT and PDT in cancer treatment induce the cell apoptosis by the enhanced temperature and cytotoxic singlet oxygen ($^1O_2$) (or ROS (reactive oxygen species)) respectively, which could not achieve effective cancer therapy individually [3]. The previous reports demonstrate the combination of PTT and PDT exhibits significant photothermally enhanced PDT efficacy by the synergistic effect, because the photothermal effect could increase intratumoral blood flow transporting more oxygen into tumor subsequently, which improve the PDT efficiency [4]. Therefore, designing novel nanoplatform with bi-function of PTT and PDT to perform the synergetic effect is the critical avenue for phototherapy of cancer.

In PDT, many photosensitizers are developed and utilized for the elimination of cancer, such as porphyrin, phthalocyanine, methylthionine chloride, hypocrellin, and titanium dioxidesetc [5–9]. As a widely used photosensitizer for PDT, titanium dioxide (TiO_2) could absorb ultraviolet (UV) light and blue light effectively, producing electrons and holes for the generation of $^1O_2$ or ROS subsequently [10]. The generated oxygen species could damage the cell membrane or DNA of cancer cells by the high reactive property at the location enriching large number of particles, which induce severe toxicity to cancer cells [11]. Despite probable outcomes for triggering apoptosis of cancer cells, the major challenge for the application of TiO_2 in PDT is that the penetration ability of UV light or blue light in tissue is limited, which cause the failure of PDT for the cancer cells locating far from the surface [12]. Thus, the designing of long-wavelength light triggered TiO_2 nanoparticles with better penetrating property to kill cancer cells

in deep tissues is a promising way to extend the application of TiO_2 nanoparticles in cancer therapy.

As an efficient method to activate the photosensitizers via fluorescence resonance energy transfer (FRET) efficacy, the upconversion materials could convert the lower energy light to higher energy light, emitting the UV or short-wavelength light effectively [13]. Surprisingly, carbon dots (CDs) are novel fluorescent materials with the upconvertable ability which could convert the long-wavelength light to short-wavelength light (blue light), achieving the utilization of bio-imaging in cancer diagnosis [14]. Synthetic approaches for CDs are generally classified into two categories: "top-down" and "bottom-up" [15]. The "top-down" methods include arc-discharged soot, laser ablation, electrochemical method and so on. On the other hand, the "bottom-up" avenues are obtained from molecular precursors such as citrate, carbohydrates, and polymer–silica nanocomposites through thermal treatments, and supported synthetic and microwave synthetic routes. Owing to the special optical property, the sensitization of TiO_2 nanoparticles by CDs is possible via the FRET effect in PDT. Moreover, CDs are excellent photothermal agents which are applied for ablating cancer cells successfully [16]. According to the reported work, the mesoporous silica nanoparticles were used as a coating material to encapsulate the graphene quantum dots and doxorubicin hydrochloride, forming the nanocomposites (DOX-GQD-MSNs) for synergistic photothermal and chemotherapy. Besides, we found that the FRET effect could induce fluorescence quenching of CDs, enhancing the photothermal property of the synthesized nanocomposites obviously [17]. Furthermore, the mesoporous silica based-nanosystems possess controlled size and shape can be varied widely to accommodate high payloads of disparate cargos [18]. The colloidal mesoporous silica is biodegradable and generally recognized as safe by the Food and Drug Administration. Hence, many kinds of mesoporous silica based-nanosystems have been developed for delivering drugs to anticancer. However, a new attempt of combining TiO_2, CDs, and SiO_2 to synthesize a
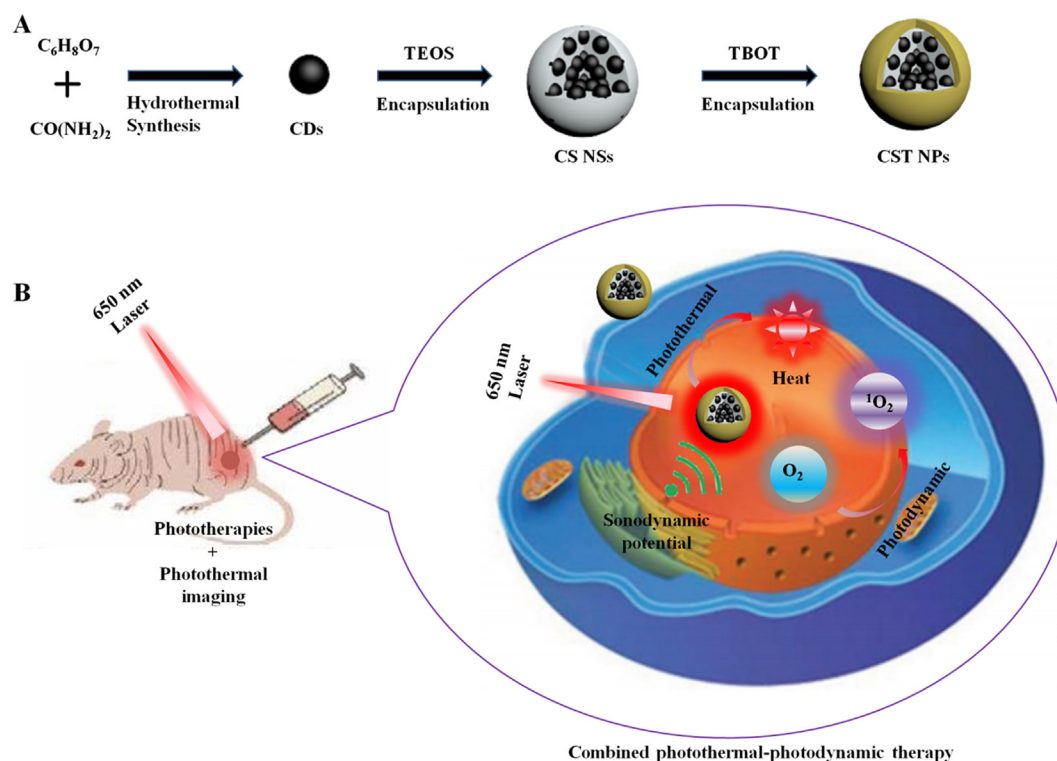

Fig. 1. The (A) synthesis and (B) simulating response of multifunctional CST NPs.

long-wavelength triggered nanoplatform for synergistic PDT and PTT is not explored.

For resolving the above-mentioned problems in cancer therapy, a multifunctional nanoplatform was designed by the combination of CDs, SiO_2, and TiO_2 with the core-shell structure (As shown in Fig. 1A). The CDs were coated with SiO_2 to form the spherical CDs@SiO_2 nanospheres (CS NSs), acting as the multifunctional core for photothermal therapy and photothermal imaging (PI). Then the synthesized CDs@SiO_2 NSs were further wrapped by TiO_2 as the shell to produce the core-shell structured CDs@SiO_2@TiO_2 nanoplatforms (CST NPs), realizing the PDT by FRET effect. For the comparison with other TiO_2-based PDT systems, the novelty of this work includes the following. (1) CST NPs possess good biocompatibility and uniform size, which are suitable for the application in cancer therapy. (2) The multifunctional core of CST NPs not only contributes for PTT and PI inducing apoptosis of cancer cells impressively, but also emits blue light advantaging to FRET effect which sensitizes TiO_2 shell availably. (3) The integrated CST NPs could absorb long-wavelength light to achieve synergistic PTT and PDT powerfully, benefitting for the cancer therapy in deep tissues. (4) The obtained CST NPs also have response under ultrasonic stimulation with the generation of ROS, harboring available prospect in the field of sonodynamic therapy to cancer. Therefore, Fig. 1B shows that the designed CST NPs are novel multifunctional nanoplatforms which could perform multimodal cancer therapy synergistically, exhibiting significant potential in cancer therapy.

Materials and methods

Materials

Urea ($CO(NH_2)_2$), ethanol, and hydrochloric acid (36.0–38.0 wt%), were purchased from Sinopharm Chemical Reagent Co., Ltd (China). Citric acid, sodium hydroxide, and 1, 3-diphenylisobenzofuran (DPBF) ($C_{20}H_{14}O$) were obtained from Sigma-Aldrich Co. LLC. Hoechst 33342, propidium iodide (PI), penicillin, streptomycin, tetraethyl orthosilicate (TEOS), (3-Aminopropyl) triethoxysilane (APTES), 3-(4,5-dimethylthiazol-2-yl)-2,5-diphenylte trazolium bromide (MTT), pancreatin solution (25 wt%), high glucose medium (DMEM), polyvinyl pyrrolidone (PVP), and fetal bovine serum (FBS) were purchased from Sangon Biotech Inc. Tetrabutyl titanate (TBOT), and ammonia (25.0–28.0 wt%) were obtained from Macklin Inc. All the agents were analytical pure and used as received without further purification. The water used in the experiments was deionized (Milipore Mili-Q grade) with resistivity of 18.0 MΩ·cm.

Characterization

UV-Vis spectra were collected by a U-3900 UV spectrophotometer (Hitachi) ranging from 200 to 800 nm with DI water as the solvent. The fluorescent spectra were measured in aqueous dispersion by a fluorescence spectrophotometer (F-4600, Hitachi). X-ray diffraction (XRD) patterns were obtained from a X-ray diffraction (DX-2700, λ = 1.5406 Å) to investigate the phases of the products. The morphology and structure of the products were observed on scanning electron microscope (SEM, Sigma 500/VP, the accelerate voltage was 5 kV) and transmission electron microscope (TEM, JEM-100SX, the accelerate voltage was 200 kV). The photothermal effects of all samples and the IR thermal images were performed with an IR thermal camera (Fluke, Everett, WA). The laser equipment (STL650T1-1.0 W) in all experiments was obtained from Beijing Stone Boyuan Laser Technology Co., Ltd. The fluorescent images were captured by an inverted fluorescence microscopy (IX83, Olympus). The sonodynamic experiments were performed

with an ultrasonic cleaning machine (40 kHz, 400 W, Kunshan Ultrasonic Instrument CO., Ltd).

Preparation of fluorescence CDs

The fluorescent CDs were synthesized in accordance with the reported literature [1].

Preparation of CDs@SiO_2 nanospheres (CS NSs)

Generally, CDs (100 mg) and PVP (1.0 g) were added into the mixture solution of ethanol and water with the volume ratio of 4:1 (total volume is of 50 mL), followed by the addition of APTES (100 μL) and ammonia water (2 mL, 25.0–28.0 wt%) [19]. After sonication for 30 min, TEOS was dropped into the mixed dispersion slowly with a 3 h agitation at room temperature (20 °C). The suspension was centrifuged (10000 r min^{-1} for 10 min) to collect the blue CS NSs. Thus, the obtained CS NSs were washed firstly by pure water (30 mL) for 3 times following by ethanol (30 mL) for another 3 times with centrifugation to remove redundant PVP and unreacted agents. Finally, the precipitations were dried by freeze-drying for 24 h.

Preparation of CDs@SiO_2@TiO_2 nanoplatforms (CST NPs)

In brief, CS NSs (50 mg) were dispersed in ethanol (100 mL) by sonication for 30 min. After that, ammonia water (1 mL) was added into the suspension under stirring violently, followed by the careful addition of TBOT (1 mL). For a reaction of 4 h, the precipitates were obtained by the centrifugation (4000 r·min^{-1}, 10 min). Finally, the precipitates were washed by pure water and ethanol for 6 times, freeze-drying subsequently for 24 h to acquire the CST NPs.

Singlet oxygen ($^1O_2$) generation detection

DPBF was used as the probe to study the photodynamic effects of CST NPs. Generally, 1 mL of mixed-solution of alcohol and water (with the ratio of 10:90) containing DPBF (0.196 mg) and 1 mL of CST NPs dispersion (0.5 mg·mL^{-1}) were mixed evenly. Subsequently, the mixture was irradiated by a 650 nm laser for 10 min. During the irradiation, the absorption intensities of the mixed dispersion at 410 nm were collected using a spectrophotometer at predefined time points (0 min and 10 min respectively). For comparison, the photodynamic effects of CS NSs were also performed by the same process. All dark groups were treated in the same way as the control groups.

Intracellular ROS determination

HepG2 cells were cultured in the dishes (35 mm) for 24 h in an atmosphere of 5% CO_2. The DMEM suspensions containing CS NSs and CST NPs (0.5 mg·mL^{-1}) were used to incubate the cells for 6 h, followed by washing cells 3 times with PBS. The control group was co-incubated without samples at the same condition. Immediately, all groups were co-incubated with 2,7-dichlorodihydro-fluorescein diacetate (DCFH-DA) (10 μmol·L^{-1}) for 50 min. The cells were further washed 3 times by PBS before and irradiated under a 650 nm laser for 3 min. The DCFH could be oxidized to the oxidization of 2, 7-dichloro-fluorescein (DCF) by the $^1O_2$ molecules, demonstrating the generation of intracellular ROS.

Cell viability assay

To determine the cell viability with or without laser treatment condition, HepG2 cells were used to evaluate the cytotoxicity of CS

NSs and CST NPs by MTT assay [20]. HepG2 cells were seeded on 96-well plates with an initial seeding density of 5×10^3 cells per well. After 24 h incubation, all wells were washed by PBS for 3 times. Subsequently, 100 μL of DMEM medium containing CS NSs and CST NPs with different concentrations of 0, 0.1, 0.2, 0.5, and 1.0 mg·mL^{-1} were added into each well respectively. With further co-incubation for 10 h, the irradiated groups were taken out for 10 min irradiation under a 650 nm laser, following by 14 h co-incubation in the incubator. Then, 100 μL of freshly prepared MTT solution (0.5 mg·mL^{-1}) was added into each well for further 4 h incubation after washing every well with PBS for 3 times. Finally, 200 μL of DMSO was added into wells dissolving the formazan crystals to measure the characteristic absorption at 490 nm by the microplate reader. The calculated cell viabilities were according to formula (1):

$$Cell\ viability = \frac{OD_{exp}\text{-}OD_{bla}}{OD_{con}\text{-}OD_{bla}} \times 100\% \qquad (1)$$

where, OD_{bla}, OD_{exp}, and OD_{con} are the optical densities of blank, experimental, and control groups respectively.

The intracellular cytotoxicity of CS NSs and CST NPs could also be evaluated by fluorescent images using Hoechst 33,342 and PI as the imaging agents. In brief, HepG2 cells were seeded into 6-well plates at a density of 5×10^4 each well and maintained in an incubator at 37 °C, 5% CO_2 for 24 h. After 3 mL of DMEM suspension containing CS NSs and CST NPs (0.5 mg·mL^{-1}) were added to each well, followed by incubating in dark. After 10 h incubation, the irradiated groups were taken out and irradiated by a 650 nm laser for 10 min following by continual incubation. After all groups were incubated for 24 h, the medium were replaced by PBS buffer. Then 0.5 mL of Hoechst 33,342 (10 μg·mL^{-1}) and 0.5 mL of PI (10 μg·mL^{-1}) were added to each well for 15 min. The final cells were washed twice with PBS and observed by an inverted fluorescence microscopy to obtain fluorescent images.

In vivo photothermal imaging

H22 (mouse hepatoma cell line) cells (1×10^7 cells) were implanted subcutaneously into the mice [21]. When the tumor volume grew up to about 1000 mm^3, 1 mL of PBS suspension containing CST NPs (2 mg·mL^{-1}) was injected into the mice intratumorally. Then, the dosed mice were irradiated by a 650 nm laser for 10 min continuously at the tumor site. The photothermal images were taken at the time points of every 1 min to evaluate the photothermal imaging ability of the obtained CST NPs. All procedures for *in vivo* experiments were performed in accordance with Fuyang Nomarl University of Science and Technology guidelines on animal care and use.

In vivo phototherapy of tumors

H22 tumor-bearing mice (tumor volume: ≈1000 mm^3) were divided into six groups (4 mice per group) randomly, and treated with PBS, PBS + Laser, CS NSs, CS NSs + Laser, CST NPs, or CST NPs + Laser, respectively [22]. Samples were intratumorally injected into the mice with the concentrations of CS NSs and CST NPs corresponding to ca. 2 mg·mL^{-1}. After 20 min post-injection, the irradiated groups were exposed under a 650 nm laser for 10 min. The tumor size was calculated by the formulation of volume=(tumor length)×(tumor width)^2/2. Body weight and tumor volume were measured every 2 days. Tumor sections were stained with hematoxylin and eosin (H&E).

Results and discussions

Morphology and structure of samples

For the morphological investigation of the CS NSs and CST NPs, the SEM and TEM images were collected. As shown in Fig. 2A, the CS NSs possess spherical structures with the uniform size, which the average diameters are about 100 nm. The formation of CS NSs is due to the addition of PVP in the reacting process, which acts as dispersant, structure-directing agent and linker [19]. Meanwhile, the CS NSs are well dispersed benefitting for the application in cancer therapy. Fig. 2B shows that the CS NSs have the similar morphology and size, which are corresponding to the results in Fig. 2A. The TEM image of CS NSs also exhibits darker area which is close to the center of the nanosphere, demonstrating that the different brightness in CS NSs is caused by the encapsulated CDs (Insert in Fig. 2B). After coating with TiO_2, the obtained CST NPs (Fig. 2C) displays the coarser surface than that of CS NSs with an enlarged diameter (ca. 150 nm). And the related TEM image in Fig. 2D clearly reveals that the synthesized CST NPs possess obvious core–shell structure with rough outer surface. The size enhancement of CST NPs is owing to the TiO_2 coating on the outer surface of CS NSs. To investigate the structure of CST NPs clearly, HRTEM image of which was obtained (Shown in Fig. 2E). The darker area in the center was the core structure combining by CDs and SiO_2, and the brighter edge closing to the center was the shell structure forming by TiO_2 with the thickness about 15 nm. Meanwhile, no crystallized structure could be found in the image demonstrating the prepared CST NPs which were combined by noncrystalline components. Furthermore, the size of the prepared CST NPs is advantageous for the enrichment in tumor sites via the enhanced permeability and retention (EPR) effect. The thermogravimetric curves of CS NSs and CST NPs were collected in Fig. 2F. Both curves displayed a slow reduction under the temperature of 150 °C, assigning to the absorbed H_2O in the samples (ca. 6.1 wt% and 7.7 wt% respectively). The fast mass loss from 150 to 650 °C were attributed to the existence of PVP and CDs in the structure of CS NSs and CST NPs with the total contents about 33.6 wt% and 22.7 wt%, respectively. The calculated SiO_2 contents in every sample were of 60.3 wt% and 40.7 wt% individually. The redundant weight in CST NPs was about 28.9% originating from TiO_2. Thus, all the aforementioned results represent the obtained CST NPs possessing compatible morphology and size, benefitting for the application in cancer therapy by passive targeting as multifunctional nanoplatforms.

To further study the elemental components and distribution of CST NPs, the elemental mappings (Fig. 3) of CST NPs were obtained. The elements of carbon (blue), silicon (violet), oxygen (yellow), nitrogen (green), and titanium (orange) are co-existence and uniformly distribute in CST NPs. Besides, the brightness of silicon, carbon, and nitrogen are concentrated in the center, and the brightness of oxygen and titanium are symmetrically distributed, which is corresponding to the merged image (Fig. 3F) of CST NPs. However, because the TEM-mapping was performed on a carbon fiber membrane, the region of carbon was full of blue. The abovementioned outcomes prove that the CST NPs are core-shell structured nanoplatforms with the $CDs@SiO_2$ core and TiO_2 shell.

For promoting confirmation of the surface elemental ingredient, XPS survey spectrum of CST NPs was applied (Fig. 4A). The characteristic peaks are observed evidently attributing to C 1s, Ti 2p, N 1s, Si 2p, and O 1s respectively, which verify the CST NPs are combined by CDs, SiO_2, and TiO_2. Further evidences come from the high-resolution spectra of C 1s, Ti 2p, N 1s, Si 2p, and O 1s, particularly. The peaks in Fig. 4B around 284.6, 285.0, 285.5, 286.4, and 287.8 eV are corresponding to the formations of C—H, C=C, C—N, C—C, and
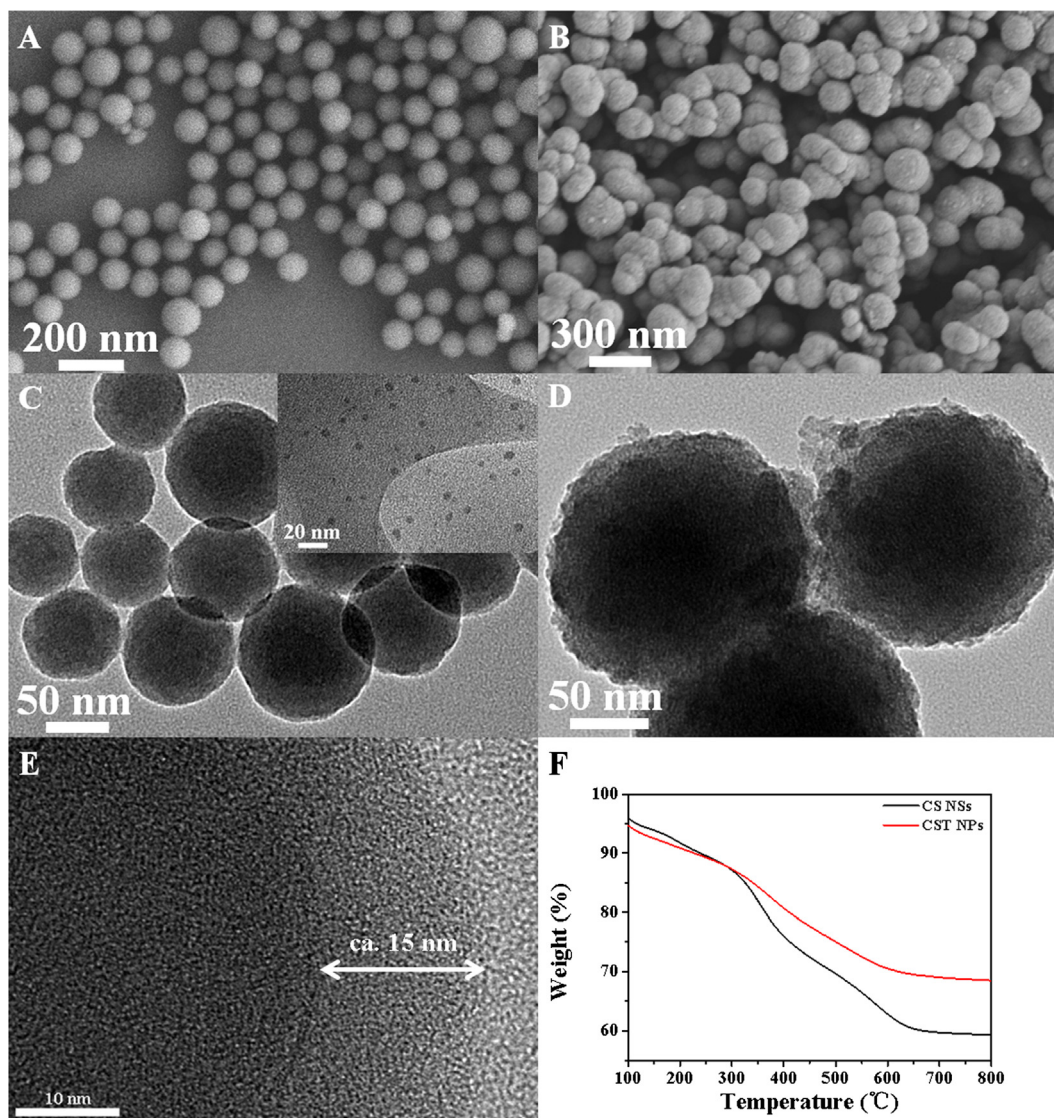
Fig. 2. SEM and TEM images of (A, B) CS NSs, and (C, D) CST NPs, respectively; (Insert in (B) is the TEM image of CDs.); (E) HRTEM image of PDA@CoPA-LA NCs; (F) Thermogravimetric of PDA@CoPA-LA NCs under air condition.

C=O bonds individually, which demonstrate the existence of CDs and PVP in the prepared CST NPs [23]. Meanwhile, the characteristic electronic states of N 1s at 399.5, 399.9, and 401.5 eV are observed clearly (Shown in Fig. 4C), which are related to N-H bond, pyrrolic N and graphitic N respectively [23]. The aforesaid indications all illustrate that the elements of C and N mainly originate from CDs integrating in the CST NPs. Fig. 4D shows the four typical peaks of Si 2p at the position of 101.5, 102.1, 102.8, and 103.4 eV, which are referred to $Si(-O)_1$, $Si(-O)_2$, $Si(-O)_3$, and $Si(-O)_4$ abbreviation systems [24]. The component of Si indicates the successful combination of CDs and SiO_2 forming CS NSs as the core of CST NPs. Moreover, the binding energy values of 458.4 and 464.1 eV related to the spin orbit pairs of Ti 2p3/2 and Ti 2p1/2 respectively (Fig. 4E), also proving TiO_2 are shell materials for the encapsulation to fabricate CST NPs [25]. Besides, more data coming from Fig. 4F display that the peaks at 529.9, 531.9, 531.2, 533.9, and 532.5 eV are attributed to the bonds of Ti—O—Ti, Ti—OH, Si—O—Si, Si—OH, and C=O particularly, which further confirm the designed CST NPs are formed by CDs, SiO_2, and TiO_2 [25–27]. All the results above verify that the prepared CST NPs are composed by the useful nanomaterials constructing multifunctional nanoplatforms.

In order to understand the combination of the designed samples, XRD patterns of CDs, CS NSs, and CST NPs are shown in Fig. 5A, individually. The broad peak at around 25.5° confirms the amorphous structure of the CDs, illustrating the low graphitization of CDs (Fig. 5A-a) [1]. Fig. 5A-b shows a wide peak at 2θ of ca. 23° which is assigned to the amorphous SiO_2 in the CS NSs [28]. Meanwhile, the peak of CDs disappears also verifying the encapsulation of CDs by SiO_2. In Fig. 5A-c, no obvious characteristic peak could be observed, which is due to that the amorphous TiO_2 packages the CS NSs as the shell forming the designed CST NPs [12]. All these results in XRD patterns of all samples prove the formation of CST NPs with core-shell structure.

Further explorations were studied by the UV-Vis spectra in Fig. 5B to investigate the optical properties of CDs, CS NSs, and CST NPs. Cure a shows the high-energy UV absorption at around 234 and 340 nm, which are assigned to π–π* transitions of sp2 hybridized carbon and n–π* transitions at the edge of the carbon lattice, respectively [29]. Especially, the CDs possess a typical absorption peak at 650 nm attributing to the generation of pyridine structure in CDs, which is corresponded to the conclusions of the XPS analysis [30]. Besides, the characteristic peaks are found
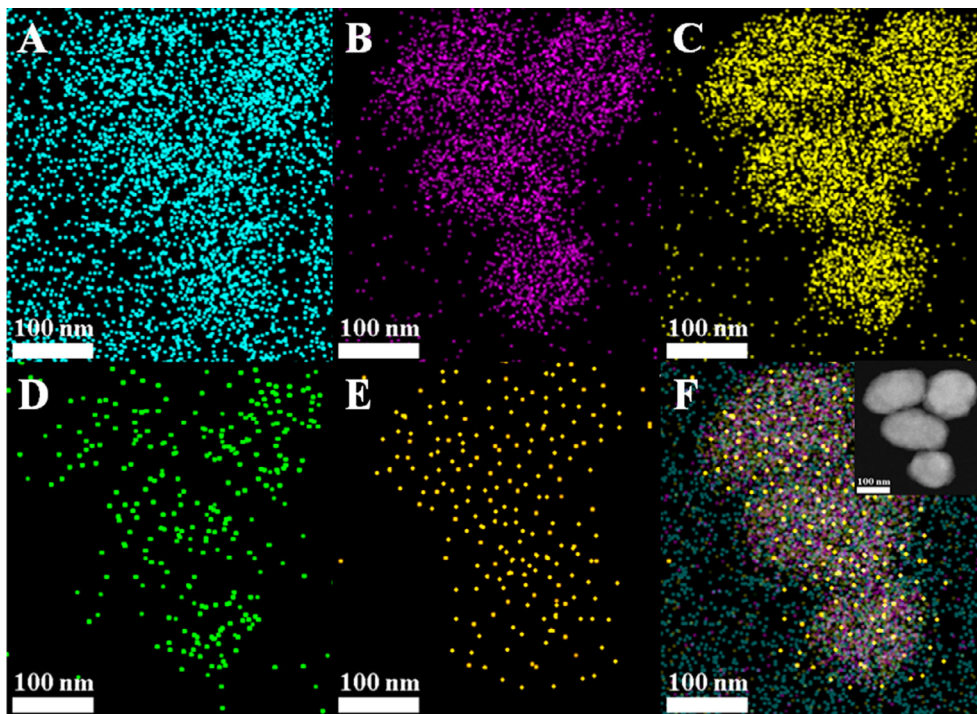
Fig. 3. Elemental mappings of (A) C, (B) Si, (C) O, (D) N, (E) Ti, and (F) Merged image of CST NPs; (The insert in (F) is the STEM image of CST NPs with the scale bar of 100 nm).

in Curve b and c too, which demonstrates the existence of CDs in the obtained CS NSs and CST NPs. The intensities of absorption bands from 200 to 300 nm and 400–550 nm are enhanced in Curve b and c, causing by the encapsulation of SiO_2 and TiO_2 individually. Interestingly, the absorption peak at 650 nm is assigned to the first near infra-red (NIR) window region with the wavelength range of 650–950 nm, which harbors high tissue penetration benefitting for PTT and PDT without damaging biological specimens and surrounding living tissues [30]. Thus, the synthesized CST NPs could absorb NIR light at 650 nm effectively to perform potential PTT and PDT.

The FRET effects of CS NSs and CST NPs are researched according to the fluorescence spectra in Fig. 5C. The CS NSs exhibits a strong fluorescence emission under the excitation at 340 nm which is attributed to characteristic fluorescent peak of CDs at 440 nm. The up-convertible property of CS NSs is investigated by the fluorescence up-conversion spectrum excited at 650 nm with the same fluorescence emission peak at 440 nm. The emitted fluorescence by up-conversion could be absorbed by CST NPs efficiently, corresponding to the absorption band in Fig. 5B-c. Moreover, CST NPs show invisible fluorescence emission under the excitation at 340 nm, which illustrates the occurrence of FRET effect between CDs and CST NPs. The abovementioned outcomes reveal existed FRET effect could induce the photodynamic efficacy of CST NPs.

To interpret the *in vitro* photothermal effect of CDs, CS NSs, and CST NPs, photothermal curves of which were performed under the same condition, using pure water as control (Fig. 5D). The temperature changes of water are ignored after a 10 min laser irradiation, demonstrating laser illumination could not induce impressive photothermal effect. Irradiating with 650 nm laser for 10 min later, the temperature enhancement of CDs (1 mg·mL^{-1}) increases about 6 °C, indicating the well photothermal effect of CDs. However, the temperature enhancement of CDs is insufficient to kill cancer cells effectually [2]. Moreover, the irradiated dispersions of CS NSs and CST NPs (1 mg·mL^{-1}) emerge remarkable temperature evolutions of ca. 19 and 21 °C respectively, which are significantly higher than that of CDs advantaging for PTT in cancer therapy. The reason is that the coated SiO_2 and TiO_2 increase the local concen-

tration of CDs, enhancing the photothermal effects of CS NSs and CST NPs. The above evidences demonstrate the designed CST NPs possess excellent photothermal performance, which is novel photothermal agent for phototherma imaging and PTT.

For further investigation of the photodynamic efficacy of CST NPs and CS NSs via FRET effect, the DPBF was used as probe to detect the generation of $^1O_2$ or ROS in the presence of CST NPs and CS NSs under the irradiation of the 650 nm laser. In Fig. 6A, the characteristic peak at 410 nm of DPBF decreases obviously after laser illumination for 10 min comparing to the initial curve at 0 min. As a contrast, the peak intensity of the group in dark displays negligible diminishment with the same laser irradiating. Meanwhile, the CS NSs dispersions were measured at the similar condition (Fig. 6B). The measurements show that the groups with laser or in dark both exhibit neglected decrease of the absorption intensity. The aforementioned results prove that the designed CST NPs are available photosensitizer for PDT application, inducing by the FRET effect between the encapsulated CDs and the coated TiO_2.

Moreover, TiO_2 is widely used as an effective sonosensitizer, which could generate ROS under sonication [31]. Thus, the synthesized CST NPs possess promising sonodynamic effect under the ultrasonic treatment (Shown in Fig. 6C and D). After sonification for 30 min, the DPBF mixed dispersion with CST NPs exhibits the obvious reduction of the typical peak intensity at 410 nm, comparing to the group without sonicating treatment. The outcome illustrates the CST NPs have outstanding sonodynamic ability. As control, the CS NSs dispersions display ignored diminishment with the same process, proving that the sonodynamic property of CST NPs originates from the coated TiO_2 shell. The above results demonstrate the designed CST NPs are potential sonosensitizers for sonodynamic therapy of cancer.

In vitro phototherapy

In order to study the intracellular ROS generation, DCFH-DA was used to estimate intracellular ROS production for the co-incubated HepG2 cells with different samples (100 μg·mL^{-1}, 6 h)
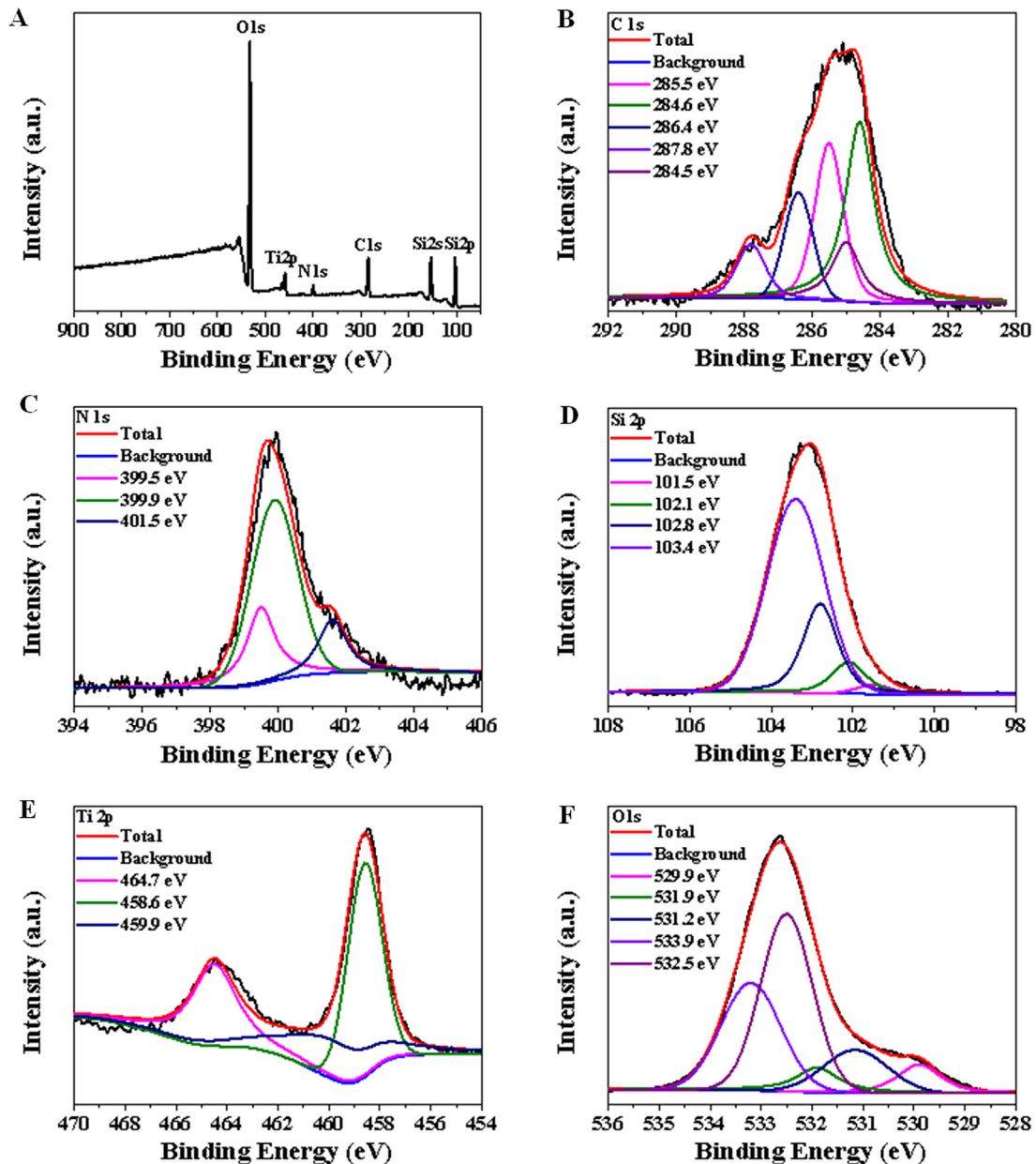
Fig. 4. (A) Survey spectrum, and high-resolution spectra of (B) C 1 s, (C) Ti 2p, (D) N 1 s, (E) Si 2p, and (F) O 1 s of the CST NPs, respectively.

[32]. The groups of control, CS NSs, and CST NPs without irradiation present all cells grow well and emit negligible DCF fluorescence, as shown in Fig. 7A-a2, 7A-b2, and 7A-c2 respectively, illustrating both CS NSs and CST NPs are biocompatible. The irradiated groups of control and CS NSs also exhibit the invisible DCF fluorescence and well growth (Fig. 7A-d2 and 7A-e2), confirming only laser irradiation or with CS NSs could not engender intracellular ROS effectively. Howbeit, the irradiated group of CST NPs displays the evident DCF green fluorescence in Fig. 7A-f2, suggests the effective creation of ROS in HepG2 cells. The previous results demonstrate that CST NPs are high performance photodynamic agents, inducing the generation of intracellular ROS for PDT in cancer.

More evidences coming from the MTT assay of CS NSs and CST NPs in Fig. 7B. The dark and irradiated groups are treated by CS NSs and CST NPs with different concentrations (0, 0.1, 0.2, 0.5, and 1.0 mg·mL^{-1}) [1]. Control groups (0 mg·mL^{-1}) with or without laser irradiation exhibit equivalent cell viabilities similarly, revealing laser irradiation could not affect the growth of HepG2 cells. The

dark groups of CS NSs and CST NPs (0.1, 0.2, 0.5, and 1.0 mg·mL^{-1}) present the cell viabilities more than 90%, which indicate that both CS NSs and CST NPs possessing favorable biocompatibility. However, the cell viabilities of HepG2 cells are about 69.3%, 58.7%, 47.8%, and 39.0% in the irradiated groups of CS NSs respectively, evidencing the powerful photothermal abilities to kill cancer cells. Moreover, the irradiated groups of CST NPs display lower cell viabilities (ca. 49.6%, 38.1%, 29.7%, and 20.9%, individually) than those of CS NSs, illustrating the enhanced cell apoptosis caused by the synergistic PTT and PDT of CST NPs. The aforementioned results prove that the designed CST NPs are available phototherapeutic agents for synergetic PTT and PDT in cancer therapy.

For further investigation of the synergistic PTT and PDT of the samples, HepG2 cells incubating with control, CS NSs and CST NPs were stained by Hoechst 33,342 (blue) and PI (red), respectively. In Fig. 7C, all dark groups show obvious blue fluorescence (a1-c1) and indiscernible red fluorescence (a2-c2), demonstrating all cells grow well with negligible cell apoptosis. Meantime, the
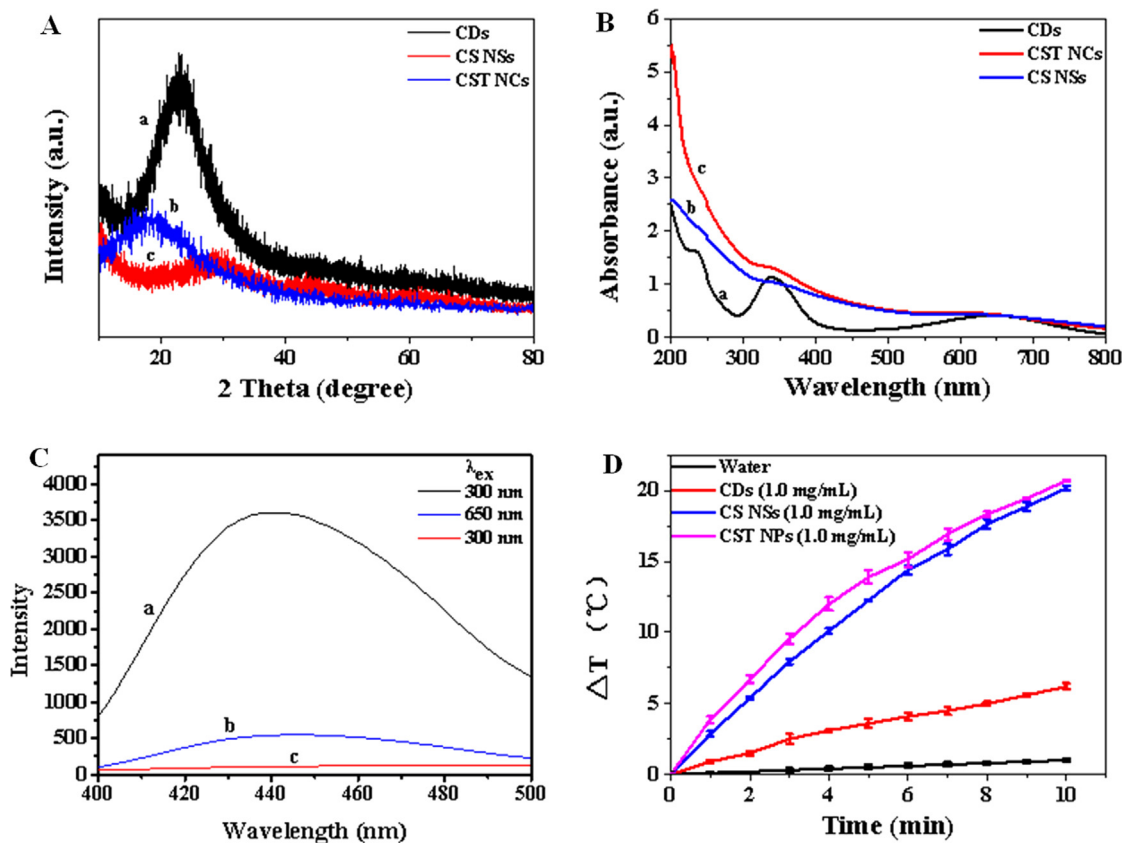
Fig. 5. (A) XRD patterns of (a) CDs, (b) CS NSs, and (c) CST NPs; (B) UV–Vis spectra of (a) CDs, (b) CS NSs, and (c) CST NPs; (C) Fluorescence spectra of (a) CS NSs, (b) up-conversion of CS NSs, and (c) CST NPs; (D) The photothermal curves of water and the dispersion of CDs, CS NSs, and CST NPs.
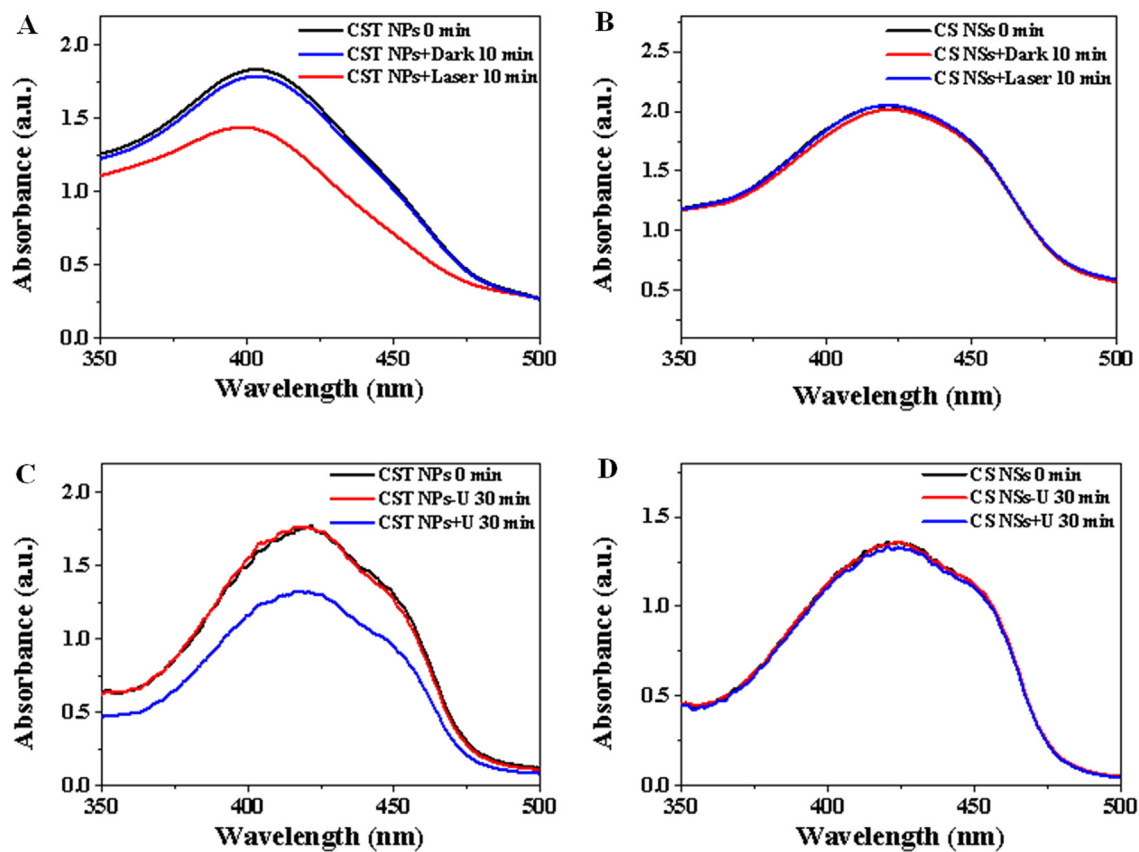

Fig. 6. Photodynamic effects of (A) CST NPs and (B) CS NSs; Sonodynamic effects of (C) CST NPs and (D) CS NSs.
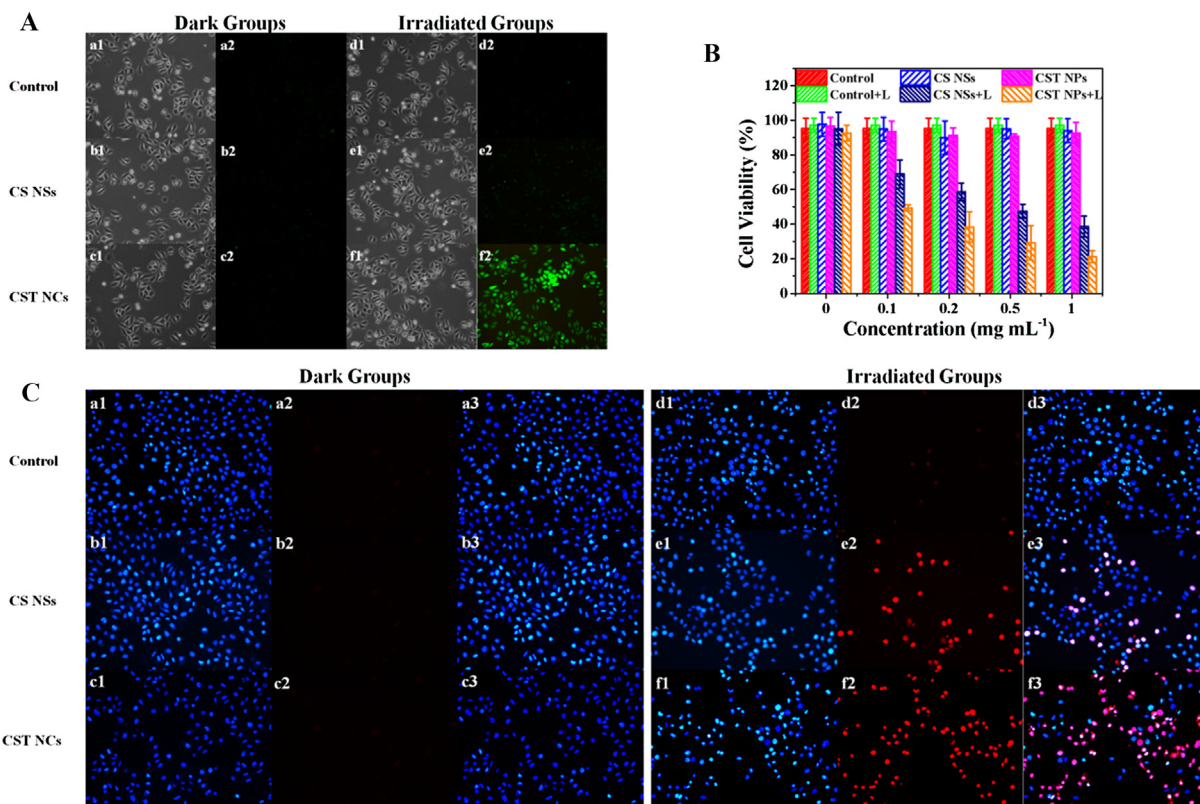
Fig. 7. (A) Intracellular ROS detections of (a, d) control groups, (b, e) CS NSs groups, and (c, f) CST NPs groups without or with laser irradiation; (B) *In vitro* MTT assay of CS NSs and CST NPs with or without laser irradiation; (C) Fluorescence imaging of (a, d) control groups, (b, e) CS NSs groups, and (c, f) CST NPs groups without or with laser irradiation. All groups were co-incubated with HepG2 cells.

irradiated group of control displays blue fluorescence (d1) and invisible red fluorescence (d2), which illustrate that the mere laser irradiating could not induce massive apoptosis of cancer cells. However, the group co-incubating with CS NSs exhibits blue fluorescence (e1) and partial red fluorescence (e2) after laser irradiation, reveals that the photothermal effect of CS NSs could kill HepG2 cells efficiently. Moreover, the irradiated group of CST NPs presents an intense red fluorescence in the merged image (f3), suggesting that the CST NPs cause severe cell apoptosis by the synergetic PTT and PDT [1]. Thus, the designed CST NPs possess excellent photoinduced therapeutic abilities for synergistic cancer therapy.

In vivo photothermal imaging

To evaluate the photothermal effect of CST NPs *in vivo*, tumor-bearing mice were irradiated by 650 nm laser for 10 min after intratumoral injection of CST NPs [33]. As shown in Fig. 8, the IR thermal images are obtained by an IR thermal mapping camera to monitor the photothermal conversion under irradiation. The mean temperature at tumor site raises nearly to 56 °C under laser irradiation for 10 min, much higher than that of the initial temperature (37 °C), revealing the excellent photothermal effect of CST NPs *in vivo*. The outstanding photothermal property of CST NPs not only benefits for photothermal therapy *in vivo*, but also advantages for real-time thermal imaging induced diagnosis and treatment of cancer.

In vivo phototherapy

In order to assess the antitumor properties of all samples *in vivo*, tumor-bearing mice were intratumorally injected with PBS, CS NSs, and CST NPs following by the treatment of laser irradiation or not [33]. From Fig. 9A, we could found that all dark groups showed a rapid increased tumor volume during 14 days, while irradiated groups displayed obvious tumor growth inhibition
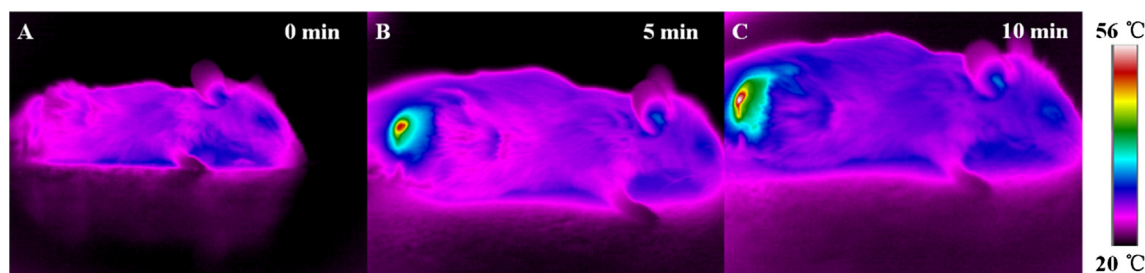

Fig. 8. *In vivo* IR thermal images of intratumoral CST NPs injected mice under constant irradiation.
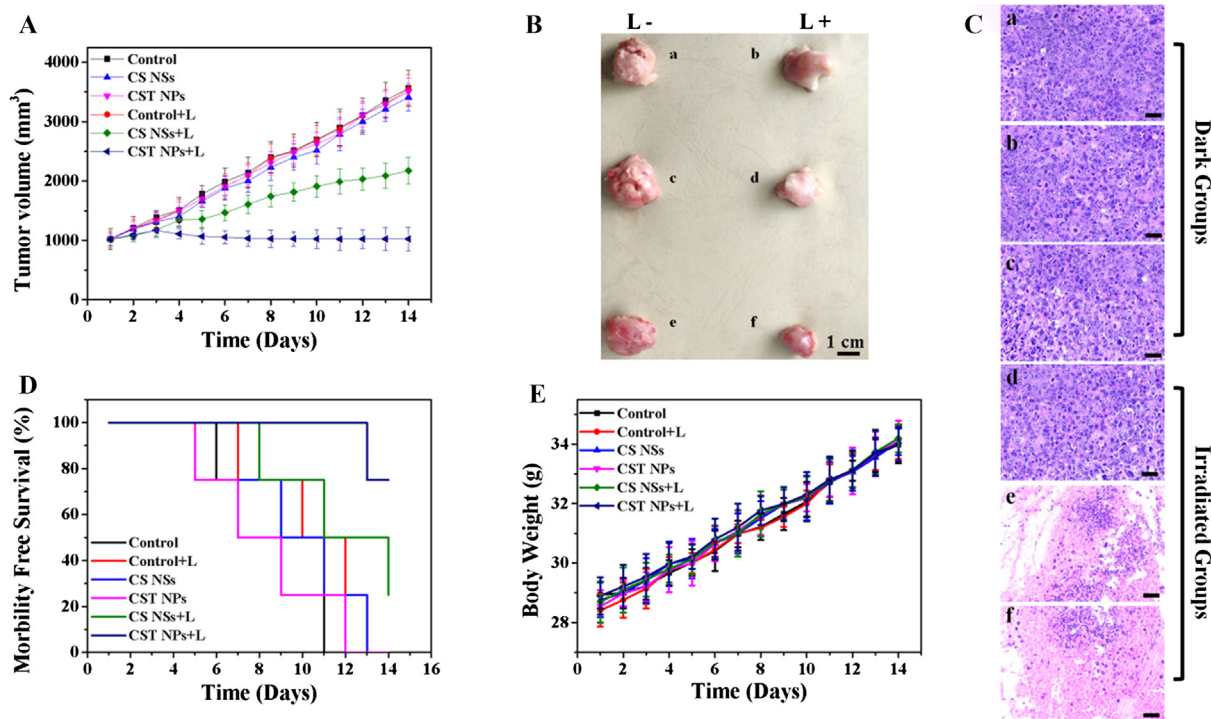
Fig. 9. *In vivo* antitumor study of (A) Tumor volumes after different treatments; (B) Representative photographs of tumor tissues treated by (a, b) PBS (Control), (c, d) CS NSs, and (e, f) CST NPs without or with laser irradiation, respectively; (C) H&E staining of tumors treated by (a, d) PBS (Control), (b, e) CS NSs, and (c, f) CST NPs without or with laser irradiation, individually (Scale bar = 100 μm); (D) Survival rates; (E) Body weight changes. (4 mice per group in all measurements).

except the saline group. This result indicates that the synthesized CS NSs and CST NPs possess excellent biocompatibility *in vivo*, and laser irradiation could activate their antitumor ability. Particularly, CST NPs + L group has smaller tumor size than that of CS NSs + L group (Fig. 9B), which is attributed to the significant synergy effects of CST NPs by PTT and PDT, and single photothermal property of CS NSs could not efficiently ablate tumor. Furthermore, the histological analyses are performed, cell nuclei are stained blue, and intracellular and extracellular proteins are stained pink [33]. As shown in Fig. 9C, obvious tumor cells damages with membrane shrinkage and nuclear condensation appear in the group of CS NSs + L (Fig. 9C-d), suggest the typical cell apoptosis. Besides, CST NPs + L group has more severe cell loss or necrosis (Fig. 9C-e), and this result further proved that the treatment of synergistic PTT and PDT is better than that of single PTT. Finally, the survival rates and body weight changes are calculated, and the results are presented in Fig. 9D and E. There is no obvious body weight loss as well as the survival rate remained at 80% for CST NPs, which demonstrate that the designed CST NPs not only have excellent phototherapeutic ability for solid tumors, but also have great biosafety *in vivo*. Therefore, the multifunctional CST NPs are considered as a promising nanoplatform for real-time thermal imaging induced diagnosis and combined PTT-PDT treatment *in vivo*.

Conclusion

In summary, we developed the novel multifunctional nanoplatforms with representative core-shell structures combining by CDs, SiO₂, and TiO₂. The designed CST NPs harbor several advantageous properties as following: (1) Suitable size and good biocompatibility are favorable for cancer therapy; (2) Excellent photothermal ability and FRET induced photodynamic property could achieve real-time thermal imaging induced diagnosis and synergetic PTT-PDT for antitumor; (3) Outstanding sonodynamic capacity endows the

CST NPs with potential sonodynamic therapy to cancer. The most important is that the synthesized CST NPs exhibit effective antitumor performance both *in vitro* and *in vivo*, owning huge prospect in clinic cancer therapy. Thus, the CST NPs are novel theranostic nanoplatforms having associative phototherapeutic ability with real-time imaging capacity, paving a new way for designing and synthesis of other multifunctional materials.

Compliance with ethics requirements

This study was conducted in strict accordance with the recommendations in the Regulations on the Management of Laboratory Animals in China promulgated in 1988. Kunming white mice that were used as a model in the present examination were purchased from the Experiment Animal Center of Anhui Medical University (Certification of quality # 34000200000077, 34000200000078). All animal studies were approved by the Institutional Animal Care and Use Committee at Fuyang Normal University (Approval No. 2013007).

Declaration of Competing Interest

The authors declare that they have no known competing financial interests or personal relationships that could have appeared to influence the work reported in this paper.

Acknowledgements

References

[1] Yang Z, Hou B, Yang Y, Jiang LX, Xie AJ, Shen YH, et al. A pH-induced charge convertible nanocomposite as novel targeted phototherapy agent and gene carrier. Chem Eng J 2018;353:350–60.

[2] Edakkattuparambil SS, Morihiko H, Norio M, Vasudevanpillai B. Nanomaterials formulations for photothermal and photodynamic therapy of cancer. J Photochem Photobiol 2013;15:53–72.

[3] Gan T, Xiao Z, Gu ZJ, Zhao YL. Recent advances in upconversion nanoparticles-based multifunctional nanocomposites for combined cancer therapy. Adv Mater 2015;27:7692–712.

[4] Bo T, Chao W, Shuai Z, Feng LZ, Zhuang L. Photothermally enhanced photodynamic therapy delivered by nano-graphene oxide. ACS Nano 2011;5:7000–9.

[5] Liang C, Anyanee K, Haiyan S, Dawei J, Hector FV, Hua G, et al. Dual-modality positron emission tomography/optical image-guided photodynamic cancer therapy with chlorin e6-containing nanomicelles. ACS Nano 2016;10:7721–30.

[6] Girgis O, Isabelle C, Michael JC, David AR. Targeting the oncofetal thomsen–friedenreich disaccharide using jacalin-PEG phthalocyanine gold nanoparticles for photodynamic cancer therapy. Angew Chem Int Ed 2012;51:6158–62.

[7] Zhe L, Waner C, Li YH, Qien X. Integrin $\alpha\nu\beta3$-targeted C-dot nanocomposites as multifunctional agents for cell targeting and photoacoustic imaging of superficial malignant tumors. Anal Chem 2016;88:11955.

[8] Ji EC, Hyun JC, Eunjue Y, Dae DK, Sanghoon J. Hypocrellin B and paclitaxel-encapsulated hyaluronic acid-ceramide nanoparticles for targeted photodynamic therapy in lung cancer. J Photochem Photobiol B 2016;158:113–21.

[9] Shi J, Chen Z, Wang B, Wang L, Lu T, Zhang Z. Reactive oxygen species-manipulated drug release from a smart envelope-type mesoporous titanium nanovehicle for tumor sonodynamic-chemotherapy. ACS Appl Mater Interf 2015;7:28554.

[10] Hu Z, Huang YD, Sun SF, Guan WC, Yao YH, Tang PY, et al. Visible light driven photodynamic anticancer activity of graphene oxide/TiO_2 hybrid. Carbon 2012;50:994–1004.

[11] Blake DM, Maness PC, Huang Z, Wolfrum EJ, Huang J, Jacoby WA. Application of the photocatalytic chemistry of titanium dioxide to disinfection and the killing of cancer cells. Sep Purif Meth 1999;28:1–50.

[12] Hou ZY, Zhang YX, Deng KR, Chen YY, Li XJ, Deng XR, et al. UV-emitting upconversion-based TiO_2 photosensitizing nanoplatform: near-infrared light mediated in vivo photodynamic therapy via mitochondria-involved apoptosis pathway. ACS Nano 2015;9:2584–99.

[13] Chen ZQ, Chen HL, He H, Yu MX, Li FY. Versatile synthesis strategy for carboxylic acid-functionalized upconverting nanophosphors as biological labels. J. Am. Chem. Soc. 2008;130:3023–9.

[14] Nelson D, Mateus BS, Ana CMM, Wagner JF, Amedea BS. Nanobiotechnology of carbon dots: a review. J Biomed Nanotechnol 2016;12:1323.

[15] Lim SY, Shen W, Gao ZQ. Carbon quantum dots and their applications. Chem Soc Rev 2015;44:362–81.

[16] Yao XX, Tian ZF, Liu JX, Zhu YF, Hanagata N. Mesoporous silica nanoparticles capped with graphene quantum dots for potential chemo-photothermal synergistic cancer therapy. ACS J Surf Colloids 2016;33:591.

[17] Yang W, Wei B, Yang Z, Sheng LQ. Facile synthesis of novel carbon-dots/hemin nanoplatforms for synergistic photo-thermal and photo-dynamic therapies. J Inorg Biochem 2019;193:166–72.

[18] Durfee PN, Lin YS, Dunphy DR, Muñiz AJ, Butler KS, Humphrey KR, et al. Mesoporous silica nanoparticle-supported lipid bilayers (protocells) for active targeting and delivery to individual leukemia cells. ACS Nano 2016;10:8325–45.

[19] Chen M, Wu L, Zhou S, You B. A method for the fabrication of monodisperse hollow silica spheres. Adv. Mater. 2006;18:801–6.

[20] Song SY, Liu Y, Zhen WY, Wang YH, Liu JH, Jin LH, et al. One-dimensional Fe_2P acted as fenton agent response to NIR II light and ultrasound for deep tumor synergetic theranostic. Angew Chemie Int Ed 2019;58:2407–12.

[21] Moon HK, Lee SH, Choi HC. In vivo near-infrared mediated tumor destruction by photothermal effect of carbon nanotubes. ACS Nano 2009;3:3707–13.

[22] Tu XL, Wang LN, Cao YH, Ma YF, Shen H, Zhang MX, et al. Efficient cancer ablation by combined photothermal and enhanced chemo-therapy based on carbon nanoparticles/doxorubicin@SiO_2 nanocomposites. Carbon 2016;97:35–44.

[23] Zhu LJ, Lu YL, Wang YQ, Zhang LQ, Wang WC. Preparation and characterization of dopamine-decorated hydrophilic carbon black. Appl. Surf. Sci. 2012;258:5387–93.

[24] Alexander MR, Short RD, Jones FR, Michaeli W, Blomfield CJ. A study of HMDSO/O_2 plasma deposits using a high-sensitivity and -energy resolution XPS instrument: curve fitting of the Si 2p core level. Appl. Surf. Sci. 1999;137:179–83.

[25] Kang XL, Song XZ, Liu S, Pei M, Wen W, Tan Z. In situ formation of defect-engineered N-doped TiO_2 porous mesocrystals for enhanced photo-degradation and PEC performance. Nanoscale Adv. 2019;1:1372–9.

[26] Kim YH, Lee DK, Cha HG, Kim CW, Kang YC, Kang YS. Preparation and characterization of the antibacterial Cu nanoparticle formed on the surface of SiO_2 nanoparticles. J Phys Chem B 2006;110:24923–8.

[27] Ivanova TM, Kochur AG, Maslakov KI, Kiskin MA, Savilov SV, Lunin VV, et al. XPS study of the electron structure of heterometallic trinuclear complexes $Fe_2M(\mu_3\text{-}O)(\mu\text{-}Piv)_6(HPiv)_3$ (MMn Co, Ni). J Electron Spectrosc Relat Phenom 2015;205:1–5.

[28] Maciej G, Aneta FS, Janusz T, Stanislaw B. Catalytic graphene formation in coal tar pitch- derived carbon structure in the presence of SiO_2 nanoparticles. Ceram Int 2018;44:3085–91.

[29] Schneider J, Reckmeier CJ, Xiong Y, Von Seckendorff M, Susha AS, Kasák P, et al. Molecular fluorescence in citric acid-based carbon dots. J Phys Chem C 2016;121:2014–22.

[30] Permatasari FA, Fukazawa H, Ogi T, Iskandar F, Okuyama K. Design of pyrrolic-N-rich carbon dots with absorption in the first near-infrared window for photothermal therapy. ACS Appl Nano Mater 2018;1:2368–75.

[31] Shen S, Wu L, Liu J, Xie M, Shen H, Qi X, et al. Core–shell structured Fe_3O_4@TiO_2-doxorubicin nanoparticles for targeted chemo-sonodynamic therapy of cancer. Int J Pharm 2015;486:380–8.

[32] Zhan N, Palui G, Safi M, Ji X, Mattoussi H. Multidentate zwitterionic ligands provide compact and highly biocompatible quantum dots. J Am Chem Soc 2013;135:13786–95.

[33] Chen WH, Luo GF, Lei Q, Hong S, Qiu WX, Liu LH, et al. Overcoming the heat endurance of tumor cells by interfering with the anaerobic glycolysis metabolism for improved photothermal therapy. ACS Nano 2017;11:1419–31.